HHS Public Access

Author manuscript

Nat Aging. Author manuscript; available in PMC 2022 October 04.

Published in final edited form as:

Nat Aging. 2021 October ; 1(10): 919–931. doi:10.1038/s43587-021-00123-6.

Effect of *APOE* alleles on the glial transcriptome in normal aging and Alzheimer's disease

Alberto Serrano-Pozo[1,2,3], **Zhaozhi Li**[1,2], **Ayush Noori**[1,2], **Huong N. Nguyen**[1], **Aziz Mezlini**[1,2,3], **Liang Li**[1], **Eloise Hudry**[1,3], **Rosemary J. Jackson**[1,3], **Bradley T. Hyman**[1,2,3], **Sudeshna Das**[1,2,3,✉]

[1]Department of Neurology, Massachusetts General Hospital, Boston, MA, USA.

[2]Massachusetts Alzheimer's Disease Research Center, Charlestown, MA, USA.

[3]Harvard Medical School, Boston, MA, USA.

Abstract

The roles of *APOE*ε4 and *APOE*ε2—the strongest genetic risk and protective factors for Alzheimer's disease—in glial responses remain elusive. We tested the hypothesis that *APOE* alleles differentially impact glial responses by investigating their effects on the glial transcriptome from elderly control brains with no neuritic amyloid plaques. We identified a cluster of microglial genes that are upregulated in *APOE*ε4 and downregulated in *APOE*ε2 carriers relative to *APOE*ε3 homozygotes. This microglia-*APOE* cluster is enriched in phagocytosis—including *TREM2* and *TYROBP*—and proinflammatory genes, and is also detectable in brains with frequent neuritic plaques. Next, we tested these findings in *APOE* knock-in mice exposed to acute (lipopolysaccharide challenge) and chronic (cerebral β-amyloidosis) insults and found that these mice partially recapitulate human *APOE*-linked expression patterns. Thus, the *APOE*ε4 allele might prime microglia towards a phagocytic and proinflammatory state through an *APOE–TREM2–TYROBP* axis in normal aging as well as in Alzheimer's disease.

✉**Correspondence and requests for materials** should be addressed to Sudeshna Das. sdas5@mgh.harvard.edu.

Author contributions

A.S.-P. conducted conceptualization, supervision, writing of the original draft, writing, review and editing and funding acquisition. Z.L. was responsible for formal analysis, software, visualization, data curation, writing, review and editing. A.N. undertook formal analysis, software, visualization, data curation, writing, review and editing. H.N.N., A.M. and L.L. conducted investigations. E.H. contributed to conceptualization. R.J.J. undertook formal analysis, supervision, writing, review and editing. B.T.H. contributed to conceptualization, resources, writing, review, editing and funding acquisition. S.D. was involved in conceptualization, methodology, supervision, resources, project administration, writing of the original draft, writing, review, editing and funding acquisition.

Code availability

Code for all data analyses is available on GitHub at https://mindds.github.io/apoe-glia.

Reporting Summary. Further information on research design is available in the Nature Research Reporting Summary linked to this article.

Additional information

Supplementary information The online version contains supplementary material available at https://doi.org/10.1038/s43587-021-00123-6.

Peer review information *Nature Aging* thanks the anonymous reviewers for their contribution to the peer review of this work.

Reprints and permissions information is available at www.nature.com/reprints.

Competing interests

The authors declare no competing interests.

Although genome-wide association studies (GWAS) have rendered dozens of new risk loci in the past decade, the apolipoprotein E (*APOE*) ε4 allele remains the strongest genetic risk factor for sporadic Alzheimer's disease (AD), and the ε2 allele the strongest protective genetic factor[1]. *APOE*ε4 carriers have approximately three (for heterozygotes) to 12 (for homozygotes) times higher risk of developing AD and an earlier age at symptom onset than *APOE*ε3 homozygotes[2]. Conversely, one *APOE*ε2 allele reduces the risk of developing AD by about 60%, and two copies of *APOE*ε2 decrease AD risk by 85% compared to *APOE*ε3 homozygotes[3]. Pathologically, the *APOE*ε4 allele is primarily associated with a higher burden of amyloid-β (Aβ) plaques and cerebral amyloid angiopathy (CAA), whereas the *APOE*ε2 allele is associated with a lower burden of both lesions[3–7]. In fact, APOE is known to deposit with Aβ in dense-core, typically neuritic, amyloid plaques and within CAA-laden vessels[8].

In the past 5 years our understanding of the role of the *APOE* genotype in AD has expanded from Aβ-centric to glial mechanisms. *APOE* is expressed and secreted by both microglia and astrocytes, which are known to react to neuritic plaques (NPs)[9–11] and to take up and degrade Aβ[12]. Previous stereology-based quantitative neuropathological studies did not detect any differences in the absolute number of reactive ($GFAP^+$) astrocytes and activated ($IBA1^+$ or $CD68^+$) microglia between *APOE*ε4 carriers and noncarrier AD subjects[9–11]. Recent transcriptomic studies, however, have shown that the molecular signatures of these glial cells differ by *APOE* genotype in mice expressing human *APOE* alleles (ε2, ε3 or ε4) within the murine *Apoe* locus[13–17] (henceforth referred to as *APOE* knock-in mice), and in human inducible pluripotent stem cell (hiPSC)-derived glial cells obtained from patients with AD[12,18,19]. Nonetheless, the effects of the various *APOE* alleles on microglial and astrocytic transcriptomic responses in the human aging and AD brain remain to be fully elucidated[20,21].

We hypothesized that the *APOE*ε4 and *APOE*ε2 alleles are associated with opposing microglial and astrocytic phenotypes, deleterious and protective, respectively. To test this hypothesis, we investigated whether *APOE* genotype influences microglial and astrocytic transcriptomic responses in the normal aging human brain, and in the context of AD (that is, at increasing levels of NPs and neurofibrillary tangles (NFTs)), in publicly available brain bulk RNA-sequencing (RNA-seq) datasets. We observed that the *APOE* genotype influences the microglial gene expression profile, with *APOE*ε4 carriers exhibiting a proinflammatory and phagocytic phenotype compared to *APOE*ε3 homozygotes, and *APOE*ε2 carriers demonstrating the opposite effect. Importantly, these differences were present in subjects with no NPs, suggesting an *APOE*ε4-mediated priming of microglia. Follow-on experiments in *APOE* knock-in mice subjected to an acute inflammatory stimulus such as lipopolysaccharide (LPS), or in the presence of chronic β-amyloidosis (that is, crossed with *APP/PS1* transgenic mice), further support this association of microglial phenotype with the *APOE*ε4 allele. In contrast to microglia, the influence of *APOE* alleles on the astrocyte transcriptome appears to be modest and suggests a dysregulation of lipid metabolism and the extracellular matrix.

Results

A graphical summary of the workflow is illustrated in Fig. 1.

APOE-linked microglial transcriptomic changes in normal aging.

Spectral clustering is useful in finding genes with similar expression profiles in large datasets by extraction of connected genes in a coexpression graph. To identify clusters of coexpressed microglial genes associated with *APOE* alleles, we performed spectral clustering on the expression levels of 519 microglia-predominant genes in the subset of control subjects with no NPs (CERAD NP score 0 or C0) from the Religious Orders Study and Memory and Aging Project (ROSMAP) dorsolateral prefrontal cortex (DLPFC) bulk RNA-seq dataset. We reasoned that genes following an ε2 < ε3 < ε4 or an ε2 > ε3 > ε4 pattern of expression level would be more likely to be regulated or influenced by the *APOE* genotype, whereas those following a ε2 ~ ε3 ~ ε4 pattern would not be related to *APOE*. Spectral clustering with $k = 3$ using the average z-score across individuals in each *APOE* group (Fig. 2a) identified a cluster with 172 coexpressed genes that are both down in *APOE*ε2 carriers (including ε2/ε3 and ε2/ε2) and up in *APOE*ε4 carriers (including ε2/ε4, ε3/ε4 and ε4/ε4) compared to *APOE*ε3 homozygotes (heatmap in Fig. 2b, violin plot in Fig. 2c). The 172 genes in this cluster, henceforth referred to as the 'microglia-*APOE* cluster', with their average z-scores for each *APOE* group of the ROSMAP C0 cohort, are available in Supplementary Table 1.

A closer inspection of this microglia-*APOE* cluster revealed a strong representation of multiple aspects of phagocytosis, including chemotaxis genes (*CCL2*, *CCL20*, *CCR1*, *CCR5*); cytoskeleton and cell motility (*ABI3*, *AIF*, *ARPC1B*, *DOCK2*, *DOCK11*, *LCP1*, *MYO1F*, *MYOF*, *PARVG, SCIN*); extracellular matrix and cell adhesion (*CLEC5A*, *CHSY1*, *EMB*, *HPSE*, *ITGAM*, *ITGB2*, *ITGB3*, *LPXN*, *NEDD9*, *PLAU*, *PLEK*, *SELL*, *SPP1*, *SRGN*, *TGFBI*, *TGFBR1*); antigen presentation (*CD14*, *CD74*, *CD86*, *CIITA*); opsonization (immunoglobulin receptor *FCER1G*, complement factors *C3*, *C1QA*, *C1QB* and *C1QC* and complement receptors *C3AR1*, *C5AR1* and *VSIG4*); scavenger receptors (*CD163*, *MSR1*); phagocytosis receptors and adapters (*TREM1*, *TREM2*, *TREML1*, *TYROBP*); autophagosome respiration burst (*CYBB*, *NCF2*, *NCF4*); and lysosomal function (*CD68*, *CPVL*, *CTSC*, *CTSS*, *LAPTM5*, *NAGA*). Additionally, this gene cluster contains numerous proinflammatory genes including interleukins and interleukin receptors (*IL10RA*, *IL13RA1*, *IL16*, *IL18BP*, *IL1R2*); Toll-like receptors (*CD180*, *TLR1*, *TLR2*, *TLR3*, *TLR7*); interferon response (*IFNGR1*, *IFNGR2*, *IRF8*); tumor necrosis factor pathway (*TNFRSF1B*, *TNFAIP8L2*); arachidonic acid metabolism (*ALOX5*, *ALOX5AP, PLA2G4A*, *PTGER4*, *PTGS1*, *PTGS2*, *TBXAS1*); and the inflammasome-associated caspase 1 (*CASP1*). Other interesting genes include the AD-linked GWAS loci *INPP5D*, *MS4A7* (within the *MS4A* cluster), *ABI3* and *PLCG2* (refs.[1,22–24]); calcium homeostasis (*S100A9* and *S100A11*); purinergic signaling (*P2RY12* and *P2RY13*); energy metabolism (*FBP1*, *PYGL* and *UCP2*); and lipid metabolism (*CH25H*).

Statistical analyses revealed a significant difference in this microglia-*APOE* cluster composite gene expression—defined as the average z-score of the 172 genes—in C0 *APOE*ε2 and *APOE*ε4 carriers versus C0 *APOE*ε3 homozygotes (*APOE*ε2 versus *APOE*ε3

estimate (s.d.), $P = -0.39$ (0.13), $P = 0.002$; *APOE*ε4 versus *APOE*ε3, 0.40 (0.18), $P = 0.025$; *APOE*ε4 versus *APOE*ε2, 0.79 (0.20), $P = 0.0001$). Application of spectral clustering on the Braak NFT 0/I/II (B1) rather than C0 subjects yielded similar results, with one cluster of similar size ($n = 200$ genes) following the ε2 > ε3 > ε4 pattern and significantly overlapping with the microglia-*APOE* cluster derived from C0 subjects ($n = 100$ genes overlapping; $P = 2.24 \times 10^{-23}$, hypergeometric test). Comparison of the composite *z*-score of this B1-derived microglia gene cluster across *APOE* genotypes revealed statistically significant differences or a trend towards statistical significance relative to *APOE*ε3 homozygotes (*APOE*ε2 versus *APOE*ε3, −0.45 (0.16), $P = 0.006$; *APOE*ε4 versus *APOE*ε3, 0.23 (0.15), $P = 0.123$; *APOE*ε4 versus *APOE*ε2, 0.69 (0.20), $P = 0.0007$).

These analyses were run in a second, independent, public gene expression dataset obtained from the Mount Sinai Brain Bank (MSBB), which includes four different brain regions. When the MSBB bulk RNA-seq study brain regions were analyzed individually, the superior temporal gyrus (STG) contained 71 genes with the ε2 < ε3 < ε4 pattern in common with the ROSMAP microglia-*APOE* cluster ($P = 5.83 \times 10^{-4}$, hypergeometric test) whereas the other brain regions (parahippocampal gyrus (PHG), inferior frontal gyrus (IFG) and frontal pole (FP)) did not show significant overlap with the ROSMAP microglia-*APOE* cluster. When RNA-seq data from these four brain regions were combined to maximize statistical power, the microglia-*APOE* cluster displayed a similar trend of change in C0 individuals across *APOE* groups (Fig. 2d and Supplementary Table 1). Specifically, *APOE*ε2 and *APOE*ε3 did not significantly differ (*APOE*ε2 versus *APOE*ε3, −0 (0.13), $P = 0.98$), but the difference between *APOE*ε4 and *APOE*ε3 subjects was marginally significant (*APOE*ε4 versus *APOE*ε3, 0.27 (0.14), $P = 0.052$).

Taken together, these data show a strong association between *APOE* alleles and the transcriptional profile of microglia in the normal aging brain without neuritic plaques, with *APOE*ε4 driving an apparent switch towards a phagocytic and proinflammatory phenotype[25,26].

*APOE*ε4-linked phagocytic/proinflammatory microglia in AD.

Next, we investigated whether microglia-*APOE* cluster genes are also present in AD brains and whether changes across *APOE* genotypes are accentuated or attenuated with increasing NP densitiy (that is, increasing CERAD NP scores). Spectral clustering applied on the ROSMAP DLPFC bulk RNA-seq expression data from individuals with frequent NP (C3) also revealed a cluster of 181 microglia-predominant genes (cluster 3) following an ε2 < ε3 < ε4 pattern. Importantly, 87 of these 181 genes (Fig. 3a) were also part of the microglia-*APOE* cluster found in the absence of NP (C0 subjects), an overlap that was statistically significant ($P = 5.5 \times 10^{-17}$, hypergeometric test). These included chemotaxis (*CCL2*, *CCR1*, *CCR5*); cytoskeleton and cell motility (*ABI3*, *ARPC1B*, *DOCK2*, *DOCK11*, *LCP1*, *MYO1F*); extracellular matrix and cell adhesion (*ITGB2*, *NEDD9*, *PLAU*, *PLEK*, *SPP1*, *SRGN*, *TGFBR1*); antigen presentation (*CD14*, *CD74*, *CIITA*); opsonization (*FCER1G*, *C1QC*, *C3AR1*, *C5AR1*, *VSIG4*); the scavenger receptor *MSR1*; phagocytosis receptors and adapters (*TREM2*, *TREML1*, *TYROBP*); autophagosome respiration burst and lysosomal function (*NCF2*, *NCF4, CTSC*, *LAPTM5*); the interleukin receptor *IL10RA*; Toll-like

receptors (*CD180*, *TLR1*, *TLR7*); the interferon-related transcription factor *IRF8*; the tumor necrosis factor pathway (*TNFRSF1B*, *TNFAIP8L2*); and arachidonic acid metabolism (*ALOX5*, *ALOX5AP*, *PTGS1*, *TBXAS1*). These 87 genes also included the AD-linked GWAS genes *INPP5D*, *MS4A7*, *ABI3* and *PLCG2* (refs.[1,22–24]), the calcium homeostasis genes *S100A9* and *S100A11* and the energy metabolism genes *PYGL* and *UCP2*.

Statistical testing confirmed a significant difference in the average expression of this gene cluster in *APOE*ε2 and *APOE*ε4 carriers versus *APOE*ε3 homozygotes within these C3 subjects (*APOE*ε2 versus *APOE*ε3, −0.45 (0.21), $P = 0.034$; *APOE*ε4 versus *APOE*ε3, 0.30 (0.10), $P = 0.003$; *APOE*ε4 versus *APOE*ε2, 0.75 (0.21), $P = 0.0005$). In parallel analyses, spectral clustering in Braak NFT V/VI stages (B3 subjects) revealed a cluster (cluster 2) of 141 genes, 99 of which overlapped significantly with the C3 cluster above ($P = 1.6 \times 10^{-35}$, hypergeometric test). When the composite expression-level *z*-score of these 141 genes was statistically compared across *APOE* groups, *APOE*ε2 carriers exhibited a trend towards significantly lower levels than *APOE*ε3 homozygotes (−0.53 (0.29), $P = 0.066$) whereas *APOE*ε4 differed significantly from *APOE*ε2 carriers (0.63 (0.29), $P = 0.032$) but not from *APOE*ε3 homozygotes (0.09 (0.11), $P = 0.378$). To determine whether these results are robust across multiple datasets and brain regions, we also performed spectral clustering on C3 subjects from the MSBB cohort. Statistical testing of the 181 ROSMAP C3 ε2 < ε3 < ε4 cluster genes in the combined MSBB data revealed significant differences between *APOE*ε4 and *APOE*ε3 carriers (*APOE*ε2 versus *APOE*ε3, −0.11 (0.16), $P = 0.504$; *APOE*ε4 versus *APOE*ε3, 0.19 (0.08), $P = 0.022$; *APOE*ε4 versus *APOE*ε2, 0.30 (0.17), $P = 0.084$). In addition, MSBB STG and IFG included many genes with the ε2 < ε3 < ε4 pattern, which overlapped significantly with the 181 ROSMAP C3 cluster genes (STG: 82 genes, $P = 2.79 \times 10^{-11}$; IFG: 87 genes, $P = 3.38 \times 10^{-16}$). In contrast, MSBB PHG and FP had very few genes exhibiting these patterns. The modest concordance between ROSMAP and MSBB brain regions (analyzed individually) could be explained, at least in part, by the small number of *APOE*ε4 carriers among C0 subjects and of *APOE*ε2 carriers among C3 subjects, which is inherent in the effect of these *APOE* alleles on AD risk.

To further confirm the associations of *APOE* genotype with microglial gene expression independent of plaques, we also performed differential expression analysis of the ROSMAP DLPFC bulk RNA-seq dataset adjusting for CERAD NP score, using *APOE* genotype as a factor and with an *APOE*ε4 allele dosage model. These models identified 117 and 185 differentially expressed genes (DEGs), respectively, with significantly increased expression in *APOE*ε4 carriers compared to *APOE*ε3 homozygotes (Supplementary Tables 2 and 3). In the dosage model, 79 genes reached study-wide significance (that is, adjusted $P < 0.05$) in the ROSMAP data and, of these, 63 were also significant (adjusted $P < 0.05$) in the combined MSBB data. Notably, *TYROBP* is significant (adjusted $P < 0.05$) in both datasets while *TREM2* is significant (adjusted $P < 0.05$) in MSBB but only nominally significant (unadjusted $P < 0.05$) in the ROSMAP data.

We next investigated whether the strength of the association between *APOE* genotype and the microglial transcriptome varies across CERAD NP scores. We hypothesized that differences in the microglial transcriptome would become more prominent in individuals with moderate (C2) or frequent (C3) cortical NPs (that is, greater fold-changes as

AD neuropathology accumulates), given the well-established response of microglia near NPs[10,11]. We focused these analyses on the 87 genes that are common between the microglia-*APOE* C0 and C3 clusters—that is, those genes which demonstrated an ε2 < ε3 < ε4 pattern in ROSMAP individuals with no or frequent NPs. Figure 3b illustrates the average expression levels of these 87 microglia-predominant genes across CERAD NP scores, split by *APOE* group. Figure 3c shows the matrix of correlation and density plots of fold-change for *APOE*ε4 versus *APOE*ε3 comparison across CERAD NP scores. Surprisingly, *APOE*-associated microglial gene expression changes were most prominent in the absence of NPs (C0) and in the presence of frequent NPs (C3), whereas these differences were attenuated between sparse (C1) and moderate (C2) NPs. Taken together, these results suggest that microglia are primed toward a proinflammatory and phagocytic phenotype in *APOE*ε4 carriers in the normal aging brain, and that these microglial responses are again exacerbated in advanced AD stages.

APOE-associated astrocyte transcriptomic changes.

Since *APOE* expression is highest in astrocytes in the normal brain[27], we also investigated *APOE* allele-associated effects on the astrocyte transcriptome in ROSMAP brains with no NPs (C0 subjects). By applying spectral clustering on the average *z*-scores of each *APOE* group for 397 astrocyte-predominant genes, we identified five clusters with distinct patterns of gene coexpression across *APOE* alleles (Fig. 4a). Clusters 1 and 4 stood out as following an ε2 > ε3 > ε4 and an ε2 < ε3 < ε4 pattern of expression, respectively (Fig. 4b–d). A closer look at cluster 1 (ε2 > ε3 > ε4, $n = 75$ genes) revealed genes involved in lipid metabolism (*ACACB*, *ACBD7*, *ACOT11*, *APOE*, *LRAT*, *MTTP*, *PLA2G5*, *PLIN1*, *PLIN5*, *TTPA*) and the extracellular matrix (*COL5A3*, *HEPACAM*, *PAPLN*, *SDC4*, *SNTA1*), the trophic factor receptors *FGFR3* and *CNTFR* and many transcription factors including *NFATC4*. Interestingly, cluster 4 (ε2 < ε3 < ε4, $n = 69$ genes) is represented also by lipid metabolism (*ABCD2*, *BBOX1*, *EHHADH*) and extracellular matrix (*DTNA*, *FREM2*, *PLOD2*, *PTN*, *SPARCL1*) genes, but also includes cytoskeleton (*CNN3*, *GFAP*, *TUBB2B*, *VAV3*), calcium homeostasis (*CAMK2G*, *SRI*, *TRPM3*), antioxidant defense (*MGST1*, *PON2*, *PON3*), immune response (*CXCL1*, *IL33*, *TNFRSF11B*) and other relevant genes including *ALDH1L1*, *AQP1*, *MAOB*, *SCARA3* and the GWAS AD risk gene *FERMT2*. Thus, while the microglia-*APOE* cluster is characterized by increased phagocytic and proinflammatory gene expression levels in *APOE*ε4 microglia, similar expression analyses of astrocyte-predominant genes in C0 brains point to a dysregulation of lipid metabolism and the extracellular matrix associated with *APOE* genotype.

In contrast to microglia, in subjects with frequent NPs (C3), spectral clustering detected only a small cluster (cluster 5) with 68 genes following an ε2 < ε3 < ε4 pattern of expression, but only nine of these 68 genes overlapped with cluster 4 derived from C0 individuals. Additionally, unlike microglia, astrocyte-predominant genes were generally not significantly differentially expressed in ROSMAP *APOE*ε4 or *APOE*ε2 carriers versus *APOE*ε3 homozygotes in either normal (C0) brains or in the presence of frequent NPs (C3 subjects). For example, in C0 subjects, statistical analyses did not reveal significant differences in cluster 1 expression across *APOE* groups whereas cluster 4 expression was significantly lower in *APOE*ε2 carriers versus *APOE*ε3 homozygotes (−0.32 (0.12), $P =$

0.006), but did not significantly differ between *APOE*ε4 and *APOE*ε3 homozygotes (0.09 (0.16), $P = 0.569$). In C3 subjects, *APOE*ε4 carriers tended to have higher expression of cluster 5 than *APOE*ε3 homozygotes (0.17 (0.09), $P = 0.069$) but *APOE*ε2 carriers did not differ from *APOE*ε3 homozygotes (−0.22 (0.20), $P = 0.268$) (Fig. 4e,f). Thus, the severity of neuropathology and, perhaps also, microglial responses, rather than the *APOE* genotype itself, appears to be the primary driver of transcriptomic changes in AD astrocytes.

Testing of microglia-*APOE* cluster in *APOE* knock-in mice.

To further test the hypothesis that expression of the *APOE*ε4 allele impacts microglial phenotype, we evaluated published transcriptomics data from *APOE* knock-in mice and performed new experimental studies on these mice.

Zhao et al.[14] investigated the effects of sex, age and *APOE* alleles in the brain transcriptome of *APOE*2, −3 and −4 knock-in mice. Only two of the 172 genes of the microglia-*APOE* cluster identified in ROSMAP C0 individuals were present in *APOE*-linked modules in this mouse study (*IL18BP* in the yellow module and *ALOX5AP* in the tan module, but no genes in the cyan or light cyan modules). Interestingly, we found a highly statistically significant overlap between our human microglia-*APOE* cluster and their reported aging-associated pink module ($P = 2.69 \times 10^{-39}$, hypergeometric test), with an overlap of 35 genes including some proinflammatory (*IFNGR1*, *IRF8*, *TLR3*) and phagocytosis genes (*CD68*, *CD74*, *CTSC*, *LAPTM5*, *TREM2*, *TYROBP*). The age-associated blue module also had a significant overlap ($P = 5.61 \times 10^{-3}$, hypergeometric test). To test the hypothesis that aging as a stimulus may impact the effect of *APOE* genotype on glial genes, we performed differential gene expression analysis on their 24-month-old mouse cohort ($n =$ 48, 24 male and 24 female). Notably, only nine genes from the microglia-*APOE* cluster were significantly increased (adjusted $P < 0.05$) in *APOE*4 versus *APOE*3 knock-in mice, including *C3* and *CD74*. In another study, Nuriel et al. conducted bulk RNA-seq on the entorhinal cortex (EC) and primary visual cortex (PVC) from 14–15-month-old *APOE*3/4 versus *APOE*3/3 knock-in mice[13]. Similarly, we found little similarity between our microglia-*APOE* cluster and differentially expressed genes from that study (EC, 21 genes including *ALOX5AP*, *C3AR1*, *CCR5*, *CD163* and *MSR1*; PVC, nine genes).

Next, we experimentally examined (via real-time quantitative polymerase chain reaction (RT–qPCR)) the expression of 16 relevant microglial and astrocytic genes in brains from *APOE* knock-in mice, including those representative of the microglia-*APOE* cluster that highlight the *APOE–TREM2–TYROBP* axis[28–30] (*C1qa*, *C3*, *Cd68*, *Cd74, Il1b*, *Msr1, Spp1, Tgfbr1, Trem2* and *Tyrobp*), the microglial homeostatic genes *Cx3cr1* and *P2ry12*, the inflammatory marker *Tnfa*, the astrocyte genes *Clu* and *Gfap* and human *APOE* as control. RT–qPCR data and results are presented in full in Supplementary Table 4.

First, we ran RT–qPCR on bulk brain RNA from 10–12-month-old *APOE*2, -3 and -4 knock-in mice and observed no significant effect of *APOE* genotype on the expression levels of any of the genes analyzed (one-way analysis of variance (ANOVA) with Tukey's post hoc test; Fig. 5a and Supplementary Fig. 1a). Gene–gene correlation analyses showed a strong positive correlation ($0.6 \leq r \leq 0.8$) between *Cx3cr1* and *C1qa* and between *Cd68*, *Trem2* and *Tyrobp* (Supplementary Fig. 2A). Thus, consistent with the RNA-seq results of Zhao et al.[14],

we confirmed that the baseline expression levels of these genes do not differ across *APOE* genotypes in mice.

Second, we tested whether the *APOE*ε4 allele is associated with a bias towards a phagocytic/proinflammatory microglial phenotype in the setting of an acute injury such as that caused by a single intraperitoneal injection of LPS[31,32]. To this end, we injected either LPS or phosphate-buffered saline (PBS) into 3–4-month-old *APOE*3 and *APOE*4 knock-in mice, euthanized them 3 h later and determined the expression levels of the above genes of interest by RT–qPCR. Two-way ANOVA with *APOE*, treatment and their interaction as factors demonstrated a statistically significant increase in *Ilb1*, *Tnfa*, *C1qa*, *C3*, *Msr1*, *Gfap* and human *APOE* in response to LPS injection, whereas levels of the homeostatic microglial genes *Cx3cr1* and *P2ry12*, as well as those of the *Trem2*-dependent genes *Cd74* and *Tgfbr1*, were significantly decreased following LPS treatment, independently of *APOE* genotype (that is, *P* value of genotype × treatment interaction: NS). Remarkably, while no significant differences were detected across *APOE* alleles in 10–12-month-old *APOE* knock-in mice, we did observe a statistically significant effect of *APOE* genotype on *Trem2*, *Tyrobp*, *P2ry12* and *Cd68* (marginal significance), with higher levels in *APOE*4 versus *APOE*3 knock-in mice at age 3–4 months, independently of treatment (Fig. 5b and Supplementary Fig. 1b). After multiple comparison correction, *Tyrobp* remained significant and *Trem2* was marginally significant (adjusted $P = 0.054$). Gene–gene correlation analyses showed a very strong positive correlation ($0.8 \leq r \leq 1.0$) between *Il1b* and *Tnfa* levels, a moderate to strong positive correlation ($0.4 \leq r \leq 0.8$) between *Trem2* and *Tyrobp*, *Trem2* and *C1qa*, between *Trem2* and *Cd68* and between *C1qa* and *Cd68* (Supplementary Fig. 2b), suggesting coregulation of these genes in microglia following LPS-induced activation.

Next, to test whether *APOE* alleles differentially affect microglial gene expression in a chronic neurodegenerative scenario, we compared the brain expression levels of the same selected genes in 12-month-old *APP*/*PS1* × *APOE*3 versus *APP*/*PS1* × *APOE*4 knock-in mice, which bear similar NPs to those found in the human AD brain. *Trem2*, *Tyrobp*, *C1qa*, *Cd68* and *Cd74* were directionally higher (marginally significant, adjusted $P < 0.1$ after multiple comparison corrections) in *APP*/*PS1* × *APOE*4 versus *APP*/*PS1* × *APOE*3 knock-in mice (Fig. 5c and Supplementary Fig. 1c). Strong correlations were again observed between *Trem2* and *Tyrobp*, as well as between several other microglia-*APOE* genes tested (Supplementary Fig. 2c), suggesting that these genes are coregulated across very different stimuli. Taken together, these mouse experiments support the idea that *APOE* regulates microglial gene expression through the *TREM2–TYROBP* axis and can bias the microglial transcriptomic phenotype in a scenario of chronic stimulation.

Discussion

Our extensive analyses of available transcriptomic data from human brains identified a cluster of microglial genes that are robustly upregulated in *APOE*ε4 carriers and downregulated in *APOE*ε2 carriers relative to *APOE*ε3 homozygotes, and are enriched in both phagocytosis and proinflammatory genes. The association with the *APOE*ε4 allele was strongest in normal, NP-free brains, suggesting that the *APOE*ε4 allele itself biases microglia toward a disease-associated state in normal aging, perhaps because genetic

influences on microglial phenotype are more readily detectable in a homogeneous sample with fewer confounding factors. This *APOE*ε4-linked transcriptomic phenotype of microglia is reminiscent of the concept of microglial priming, defined as a predisposition of microglia towards an exaggerated response following a secondary stimulus[33,34], and may in turn exacerbate microglial responses to central nervous system (CNS) lesions such as the NPs and NFTs defining AD. Indeed, although *APOE*-linked differences were also detectable in AD brains, they were not linearly related to the extent of neuropathological alterations and were apparent only in advanced AD (C3) brains. One possible explanation for this is that the wide variety of AD-related brain changes that can impact the microglial activation state—such as neuronal loss, synaptic loss, NFT development and astrocyte reaction—are probably more heterogeneous in intermediate stages (C1 and C2), thus masking the *APOE* genotype-specific microglial signature, whereas in advanced AD (C3) these other stimuli may have plateaued, allowing the re-emergence of the *APOE*-microglia gene signature. Another possibility is that two major waves of microglial activation occur along the course of AD—the first as deposition of Aβ plaques takes place and the second against the pervasive neurofibrillary degeneration—as has been suggested by a neuropathological quantitative study[11] and one involving longitudinal multimodal positron emission tomography (PET) imaging (Aβ, tau and TSPO-based PET for glial responses)[35].

It is noteworthy that not only inflammation, but virtually all aspects of phagocytosis, were represented in this microglia-*APOE* cluster: chemotaxis, migration, opsonization, antigen presentation, phagocytosis, autophagosome burst respiration and lysosomal degradation. These observations raise a puzzle: glial uptake is thought to be one of the major Aβ clearance pathways and hence the upregulation of phagocytosis is expected to enhance Aβ clearance, yet the *APOE*ε4 allele correlates with a higher Aβ burden in both in vivo amyloid PET imaging[5] and postmortem neuropathological studies[3,4,6]. However, the *APOE*ε4-associated upregulation of microglial phagocytosis genes might be insufficient to overcome the proaggregant effects of APOE4 on Aβ[36–38] and/or APOE4 may lead to defective Aβ uptake and degradation by microglia[12,18]. Moreover, APOE4 may lead to deleterious phenotypes via enhanced phagocytosis of other substrates. For example, *C1Q* and *C3* have been involved in tagging of synapses for elimination by microglia in AD mouse models[39–42], and synaptic loss is the strongest correlate of the severity of cognitive impairment in AD[43]. Thus, *APOE*ε4 microglia may be more actively engulfing synapses than *APOE*ε2 or *APOE*ε3 microglia, which would result in an earlier age of cognitive decline—a well-known correlate of the *APOE*ε4 allele—and a faster rate of cognitive decline after symptom onset, which we and others have reported[44–46].

Also, our microglia-*APOE* signature notably includes both *TREM2* and *TYROBP*, which highlights the importance of the *APOE–TREM2–TYROBP* axis. *TREM2* loss-of-function mutations have been associated with a two- to threefold increased risk of developing AD[47,48]. Both *APOE* and *TREM2* are important in the phenotypic switch from homeostatic to AD-associated microglia[28–30]. AD-linked *TREM2* loss-of-function mutations and *Trem2* deletion in AD transgenic mice lead to Aβ plaques that are less compact and more neuritic, and have less microglial coverage[49–51], whereas their effects on tau NFT pathology remain controversial[52–54]. Although a phenocopy of these Aβ plaque features has been reported in AD transgenic mice following *Apoe* deletion[55], dense-core Aβ plaques do not

differ in size, microglial coverage or neuritic change per plaque between AD *APOE*ε4 carriers and noncarriers[10,11,56]. On the other hand, *TYROBP* encodes the adapter protein DAP12, which binds the intracellular domain of TREM2, CD33 and complement receptor 3 (CR3) to mediate their intracellular signal transduction, and is a key regulator of an immune- and microglia-specific network of genes involved in pathogen phagocytosis[26]. Importantly, *Tyrobp* genetic deletion in β-amyloidosis and tauopathy transgenic mice is neuroprotective, despite lessening plaque compaction and microglia coverage in the former and increasing phospho-tau levels in the latter[57,58]. By contrast, *Tyrobp* overexpression in microglia reduces Aβ plaque burden but also increases phospho-tau burden[59]. Thus, the observed differences in *TREM2* and *TYROBP* expression levels across *APOE* genotypes in aged control individuals (higher in *APOE*ε4 carriers and lower in *APOE*ε2 carriers versus *APOE*ε3 homozygotes) could have crucial implications for microglial phenotype, AD pathology and downstream neurodegeneration.

Among the proinflammatory microglial genes upregulated in *APOE*ε4 carriers, Toll-like receptors (*TLR1*, *TLR2* and *TLR3*) and caspase-1 (*CASP1*) stand out. Of note, an LPS challenge was reported to increase the secretion of cytokines, including IL-1β, in *APOE*4 versus *APOE*2 and *APOE*3 knock-in mice[60], and IL-1β levels were also higher in *APOE*4 knock-in AD transgenic mice compared to *APOE*2 and *APOE*3 knock-in AD mice[61]. An *APOE*ε4-driven microglial neuroinflammation phenotype has been implicated in accelerated neurodegeneration downstream of tauopathy[15,16]. Both caspase-1 (*CASP1*) and IL-1β are key components of the NLRP3 inflammasome, which can drive tau pathology following activation[62]. In addition, the interferon response was represented in our microglia-*APOE* cluster by *IRF8* and the interferon-γ receptors 1 and 2 (*IFNGR1* and *IFNGR2*, respectively). *IRF8* encodes the transcription factor interferon regulatory factor 8, which plays a role in switching microglia to a reactive phenotype in peripheral nerve injury[63–65] and was found to be upregulated in AD microglia in a single-nucleus RNA-seq study[30].

The association of *APOE* alleles with astrocyte transcriptome appears more modest in comparison with microglia, as judged by the relative number of DEGs for each glial cell type, but suggested a dysregulation of lipid metabolism and extracellular matrix genes in *APOE*ε4 and *APOE*ε2 carriers versus *APOE*ε3 homozygotes, resembling that found in hiPSC-derived glial cells from *APOE*ε4 versus *APOE*ε3 homozygote individuals[19]. However, the severity of AD pathology had a greater effect on the astrocyte transcriptome than *APOE* genotype.

The comparisons of our human microglia-*APOE* cluster with available RNA-seq data from *APOE* knock-in mice[13,14] rendered very little overlap. Some authors have reported considerable overlap between bulk brain transcriptomic changes in human AD brains and AD mouse models[66] and that human and mouse microglial transcriptomes are largely conserved[67], while others have found little to no concordance[68]. Therefore, we attempted to cross-validate our microglia-*APOE* signature in *APOE* knock-in mice both with and without stimulus (acute and chronic) via RT–qPCR of relevant genes. While no significant differences across genotypes were observed in the expression levels of the genes analyzed across adult (10–12-month-old) *APOE* knock-in mice, we did confirm a significant increase in *Tyrobp* and *Trem2* levels in young *APOE*4 versus *APOE*3 knock-in mice (regardless

of PBS or LPS treatment), and in adult *APP/PS1* × *APOE*4 versus *APP/PS1* × *APOE*3 knock-in mice (although differences in plaque burden between the latter pair might have contributed to these findings). Nonetheless, these results support the relevance of the *APOE–TREM2–TYROBP* axis in the transcriptomic programs activated by microglia in response to a stimulus[32].

It is tempting to speculate that the microglia-*APOE* gene signature identified in aged brains with no NPs is the result of the cumulative effect of various other insults over the course of the individual's lifetime (for example, traumatic, infectious, ischemic and so on) on microglia primed by the *APOE*ε4 genetic background. It is also very intriguing that *APOE*ε4 appears to be the evolutionarily conserved allele, with the definitive ε4 site present in the nonhuman primate[69]. Although corresponding changes in the Arg61 site cast uncertainty about the physiological effects of the Arg112 site in the nonhuman primate, our data raise the question of whether a proinflammatory/phagocytic bias of microglia might carry an evolutionary advantage—for example, fighting CNS infections, removal of neuronal debris after traumatic brain injuries or engulfing and phagocytosing synapses and axons for neural circuit refinement during development. Further studies, perhaps at single-cell resolution, of the nonhuman primate brain may help address this question.

Our study has certain limitations inherent to bulk RNA-seq data. Although it is tempting to ascribe DEGs to gains and losses in the corresponding cell functions, neurodegeneration in AD is associated with shifts in cell subpopulations (for example, decreased proportions of neurons and increased proportions of glial cells) that could explain, at least partially, the observed changes in gene expression levels. Cell-type deconvolution methods are being developed to address this issue[70,71]. However, our microglia-*APOE* signature was obtained from subjects with no NPs, implying no overt neurodegeneration other than that associated with normal aging, and therefore limited cell-type shifts. Our cell-type gene assignment, based on the application of expression-level cutoffs to a publicly available transcriptomic dataset of immunopanned cell subpopulations from the human normal brain[72], provided robust microglia- and astrocyte-enriched gene sets. Nevertheless, some genes are expressed by more than one cell type and their transcripts may go up or down in one or another cell type in the disease scenario (for example, *C3* and *APOE* itself), and disambiguation of these cell-type-specific changes would require single-cell or single-nucleus transcriptomics data.

In summary, contrasting aging and AD highlights several important biological functions that appear to be different in microglia from *APOE*ε4 and *APOE*ε2 carriers, plausibly correlating with their effect on relative risk for AD, age of onset and even rate of clinical progression. For example, the upregulation of phagocytosis and inflammation gene sets may well place *APOE*ε4 microglia in a predisposition state to react to Aβ plaques and NFTs, as well as to inflammatory and other noxious stimuli. Ultimately, large-scale, single-nucleus RNA-seq of human brains across different stages of AD pathology and *APOE* genotypes will be required to confirm the influences of the different *APOE* alleles on glial gene expression programs, and to fully understand how they relate to both AD pathology and clinical progression.

Methods

Bulk brain RNA-seq datasets.

For human data we used the RNA-seq dataset from ROSMAP as the discovery dataset[73] and the MSBB RNA-seq dataset as the validation dataset[74], which were downloaded from the Accelerating Medicines Partnership–Alzheimer's Disease (AMP-AD) Knowledge Portal (nos. syn3388564 and syn3157743, respectively). Brie y, ROSMAP data consist of fragments per kilobase exon of transcript per million mapped reads (FPKM) from DLPFC (Brodmann Area 9) of $n = 635$ subjects and were adjusted for age, sex and postmortem interval (PMI) using a linear model. The MSBB study provides a trimmed mean of *M*-values (TMM) from multiple brain regions (IFG, $n = 222$; STG, $n = 240$; FP, $n = 261$; and PHG, $n = 215$), which are already adjusted for batch, sex, race, age at death, PMI, RNA integrity number, exonic rate and ribosomal RNA rate. Both *APOE* genotype and clinical and neuropathological data were available for both datasets. The MSBB data across brain regions were combined using the *combat* function in the *sva* package in R to adjust for batch or brain region effects. Details of these two cohorts are presented in Table 1 and Supplementary Table 5, respectively.

We also used the following mouse datasets for comparison with human results: a whole-brain bulk RNA-seq study on *APOE*2, *APOE*3 and *APOE*4 knock-in mice[14] downloaded from the AMP-AD Knowledge Portal (no. syn15682620) and bulk RNA-seq data from entorhinal and primary visual cortex of 14–15-month-old *APOE*3/3 and *APOE*3/4 knock-in mice[13] downloaded from the Gene Expression Omnibus (no. GSE102334).

Gene expression analysis.

To assign genes to the appropriate cell type—microglia or astrocytes—we took advantage of the transcriptomic database of human brain cell subpopulations developed by the Barres laboratory using the immunopanning technique[72]. We considered a gene microglial (or astrocytic) if its level of expression was ≥1.5-fold higher in microglia (or astrocytes) relative to the sum of its expression in all other cell types—that is, neurons, oligodendrocytes, endothelial cells and astrocytes (or microglia). We removed lowly expressed genes (FPKM < 0.1). These criteria rendered 519 microglia-predominant and 397 astrocyte-predominant genes (Supplementary Table 6).

Because activated microglia and reactive astrocytes in the AD brain cluster within and around dense-core NPs[9–11], subjects were classified according to their CERAD NP score —that is, none (C0), sparse (C1), moderate (C2) and frequent (C3) NPs[75]—and their microglial and astrocytic transcriptomes were compared across *APOE* genotypes within each of these CERAD NP scores. Similar analyses were performed using the Braak NFT staging system[76].

We performed two separate analyses: spectral clustering and differential expression analysis. Spectral clustering is a dimensionality-reduction technique that uses the similarity matrix of the data, in this case the relative similarity of the expression-level data (average *z*-scores of all individuals in each *APOE* group) for each pair of genes, to identify clusters of coexpressed genes. Spectral clustering was performed using the *SNFtool* package[77]. We also

tested the average *z*-score of cluster genes using a linear model. DEGs were identified using *limma*[78] as those with a statistically significant difference in expression level (unadjusted $P < 0.05$) between the *APOE*ε4 or *APOE*ε2 group with the *APOE*ε3 homozygotes as reference group, after adjusting for CERAD NP score (or Braak NFT stage), as shown below:

$$\text{Expression} = \beta_0 + \beta_1 \times APOE + \beta_2 \times \text{CERAD (or Braak)} + \varepsilon$$

The *APOE*ε4 group comprised ε2/ε4, ε3/ε4 and ε4/ε4 subjects whereas the *APOE*ε2 group consisted of ε2/ε2 and ε2/ε3 individuals. We included *APOE*ε2/ε4 carriers within the *APOE*ε4 group given the genetic evidence regarding the dominant effect of the ε4 allele over the ε2 (refs.[3,6]). Multiple comparison corrections were performed using the Benjamini–Hochberg method[79]. Plots were generated using *ggplot2*, and heatmaps with *pheatmap* packages.

Animals.

We used three groups of *APOE* knock-in mice expressing human *APOE*ε2, *APOE*ε3 or *APOE*ε4 in the locus of the murine *Apoe* gene[80]. A group of 10–12-month-old mice were euthanized by CO_2 asphyxiation, perfused with ice-cold PBS and their brain tissue was collected for RNA purification and RT–qPCR. Another group, of 3–4-month-old mice, were injected intraperitoneally with either LPS (1 g kg^{-1}) or PBS as control, then euthanized by CO_2 asphyxiation 3 h following the injection. The final mouse group was created by backcrossing *APP*/*PS1* transgenic mice[81], which develop plaques at around 6 months of age, with *APOE*3 or *APOE*4 knock-in mice. These *APP*/*PS1* × *APOE* knock-in mice, aged 10–12 months, were then euthanized by CO_2 asphyxiation, perfused with ice-cold PBS and brains were collected for RT–qPCR. Each group included a total of eight mice (four males and four females), and no statistical method was used to predetermine sample size. Mice were housed in an animal facility with controlled conditions of temperature and humidity, 12/12-h dark/light cycle and ad libitum access to food and water. All animal experiments were approved by the Massachusetts General Hospital Subcommittee on Research Animal Care following the guidelines set forth by the National Institutes of Health Guide for the Care and Use of Laboratory Animals (no. 2006n000178).

RT–qPCR.

RNA was extracted from a slice of forebrain using the RNeasy Mini Kit (Qiagen) and eluted in 80 µl of nuclease-free water. RNA concentration was assessed using the DeNovix DS-11 spectrophotometer (DeNovix) and diluted to a standard concentration of 7.1 ng $µl^{-1}$ for each sample. RNA was retrotranscribed to complementary DNA using the QuantiTect Reverse Transcription kit (Qiagen). RT–qPCR was conducted with RT^2 SYBR Green Mastermix fluorescent dye (Qiagen) and QuantiTect primers (Qiagen), as listed in Supplementary Table 7, in the BioRad CFX96 Real-Time Detection System. The sequence began with a 10-min incubation at 95 °C to activate the DNA polymerase enzyme. Fluorescence data collection then commenced with 40 cycles of alternating 15 s at 95 °C and 60 s at 60 °C. Each mouse RNA sample was run in duplicate, and the average expression was computed. The ΔΔCt

relative quantification method was used to calculate gene expression. *Gtf2b* and *Gapdh* were used as housekeeping genes included in the RT^2-Profiler array to normalize for RNA amount. Briefly, the geometric mean of Ct values of these reference genes was calculated for each mouse and subtracted from the Ct value of each target gene, yielding ΔCt values. For each gene, the average ΔCt value in *APOE*3 knock-in mice (or, for mice subjected to LPS versus PBS stimulus, the average ΔCt value in *APOE*3 knock-in PBS-treated mice) was then subtracted from each sample's ΔCt value to obtain ΔΔCt values. The relative quantification (RQ) value was calculated as $2^{-\Delta\Delta Ct}$.

Statistics and reproducibility.

Expression data (ΔCt) from RT–qPCR experiments were analyzed with one-way ANOVA for the untreated 10–12-month-old *APOE* knock-in mice and *APP*/*PS1* × *APOE* knock-in mice, followed by a post hoc Tukey honestly significant difference (HSD) test. We applied two-way ANOVA with the terms genotype, treatment and genotype × treatment interaction for the 3–4-month-old LPS- versus PBS-treated *APOE* knock-in mice, followed by a post hoc Tukey HSD test. The statistical significance level was set at $P < 0.05$. Multiple comparison corrections were performed using the Benjamini–Hochberg method[79]. Outliers were detected using the Grubbs test and excluded from analyses. Gene–gene correlations were computed using Spearman's correlation, and the resulting correlation coefficients were used to generate heatmaps followed by hierarchical clustering. All analyses were performed in R v.4.0.2.

Supplementary Material

Refer to Web version on PubMed Central for supplementary material.

Acknowledgements

The results published here are in whole or in part based on data obtained from the AD Knowledge Portal (https://adknowledgeportal.org). ROSMAP data were provided by the Rush Alzheimer's Disease Center, Rush University Medical Center, Chicago, IL, USA. Data collection was supported through funding by NIA grant nos. P30AG10161 (ROS), R01AG15819 (ROSMAP; genomics and RNA-seq), R01AG17917 (MAP), R01AG30146, R01AG36042 (5hC methylation, ATAC-seq), RC2AG036547 (H3K9Ac), R01AG36836 (RNA-seq), R01AG48015 (monocyte RNA-seq), RF1AG57473 (single-nucleus RNA-seq), U01AG32984 (genomic and whole-exome sequencing), U01AG46152 (ROSMAP AMP-AD, targeted proteomics), U01AG46161(TMT proteomics), U01AG61356 (whole-genome sequencing, targeted proteomics, ROSMAP AMP-AD), the Illinois Department of Public Health (ROSMAP) and the Translational Genomics Research Institute (genomic). Additional phenotypic data can be requested at www.radc.rush.edu. MSBB data were generated from postmortem brain tissue collected through the Mount Sinai VA Medical Center Brain Bank and were provided by E. Schadt from Mount Sinai School of Medicine. This work was supported by the National Institute on Aging (nos. K08AG064039 to A.S.-P., T32AG000222-27 to R.J.J. and P30AG062421 to S.D. and B.T.H.), the Alzheimer's Association (nos. AACF-17-524184 and AACF-17-524184-RAPID to A.S.-P.), the JPB Foundation (to B.T.H.) and the Jack Satter Foundation (to A.S.-P. and S.D.).

Data availability

ROSMAP and MSBB RNA-seq data are available from the AMP-AD Knowledge Portal (https://doi.org/10.7303/syn3388564 and https://doi.org/10.7303/syn3157743, respectively). Mouse RNA-seq data from Zhao et. al. are available at the AMP-AD Knowledge Portal (https://doi.org/10.7303/syn20808171), and those from Nuriel et al. at Gene Expression

Omnibus (no. GSE102334). The data from our *APOE* knock-in mice are available in Supplementary Table 4.

References

1. Kunkle BW et al. Genetic meta-analysis of diagnosed Alzheimer's disease identifies new risk loci and implicates Aβ, tau, immunity and lipid processing. Nat. Genet 51, 414–430 (2019). [PubMed: 30820047]
2. Yamazaki Y, Zhao N, Caulfield TR, Liu C-C & Bu G Apolipoprotein E and Alzheimer disease: pathobiology and targeting strategies. Nat. Rev. Neurol 15, 501–518 (2019). [PubMed: 31367008]
3. Reiman EM et al. Exceptionally low likelihood of Alzheimer's dementia in APOE2 homozygotes from a 5,000-person neuropathological study. Nat. Commun 11, 667 (2020). [PubMed: 32015339]
4. Serrano-Pozo A, Qian J, Monsell SE, Betensky RA & Hyman BT APOEε2 is associated with milder clinical and pathological Alzheimer disease. Ann. Neurol 77, 917–929 (2015). [PubMed: 25623662]
5. Ossenkoppele R et al. Prevalence of amyloid PET positivity in dementia syndromes: a meta-analysis. JAMA 313, 1939–1949 (2015). [PubMed: 25988463]
6. Goldberg TE, Huey ED & Devanand DP Association of APOE e2 genotype with Alzheimer's and non-Alzheimer's neurodegenerative pathologies. Nat. Commun 11, 4727 (2020). [PubMed: 32948752]
7. West HL, Rebeck GW & Hyman BT Frequency of the apolipoprotein E epsilon 2 allele is diminished in sporadic Alzheimer disease. Neurosci. Lett 175, 46–48 (1994). [PubMed: 7970208]
8. Serrano-Pozo A, Das S & Hyman BT APOE and Alzheimer's disease: advances in genetics, pathophysiology, and therapeutic approaches. Lancet Neurol. 20, 68–80 (2021). [PubMed: 33340485]
9. Serrano-Pozo A et al. Reactive glia not only associates with plaques but also parallels tangles in Alzheimer's disease. Am. J. Pathol 179, 1373–1384 (2011). [PubMed: 21777559]
10. Serrano-Pozo A et al. Differential relationships of reactive astrocytes and microglia to fibrillar amyloid deposits in Alzheimer disease. J. Neuropathol. Exp. Neurol 72, 462–471 (2013). [PubMed: 23656989]
11. Serrano-Pozo A, Betensky RA, Frosch MP & Hyman BT Plaque-associated local toxicity increases over the clinical course of Alzheimer disease. Am. J. Pathol 186, 375–384 (2016). [PubMed: 26687817]
12. Lin Y-T et al. APOE4 causes widespread molecular and cellular alterations associated with Alzheimer's disease phenotypes in human iPSC-derived brain cell types. Neuron 98, 1141–1154 (2018). [PubMed: 29861287]
13. Nuriel T et al. The endosomal–lysosomal pathway Is dysregulated by APOE4 expression in vivo. Front. Neurosci 11, 702 (2017). [PubMed: 29311783]
14. Zhao N et al. Alzheimer's risk factors age, APOE genotype, and sex drive distinct molecular pathways. Neuron 106, 727–742 (2020). [PubMed: 32199103]
15. Shi Y et al. ApoE4 markedly exacerbates tau-mediated neurodegeneration in a mouse model of tauopathy. Nature 549, 523–527 (2017). [PubMed: 28959956]
16. Shi Y et al. Microglia drive APOE-dependent neurodegeneration in a tauopathy mouse model. J. Exp. Med 216, 2546–2561 (2019). [PubMed: 31601677]
17. Fitz NF et al. Trem2 deficiency differentially affects phenotype and transcriptome of human APOE3 and APOE4 mice. Mol. Neurodegener 15, 41 (2020). [PubMed: 32703241]
18. Konttinen H et al. PSEN1ΔE9, APPswe, and APOE4 confer disparate phenotypes in human iPSC-derived microglia. Stem Cell Rep. 13, 669–683 (2019).
19. Julia TCW et al. Cholesterol and matrisome pathways dysregulated in human APOE ε4 glia. Preprint at bioRxiv 10.1101/713362 (2019).
20. Olah M et al. A transcriptomic atlas of aged human microglia. Nat. Commun 9, 539 (2018). [PubMed: 29416036]
21. Lefterov I et al. APOE2 orchestrated differences in transcriptomic and lipidomic profiles of postmortem AD brain. Alzheimers Res. er 11, 113 (2019).

22. Conway OJ et al. ABI3 and PLCG2 missense variants as risk factors for neurodegenerative diseases in Caucasians and African Americans. Mol. Neurodegener 13, 53 (2018). [PubMed: 30326945]
23. Sims R et al. Rare coding variants in PLCG2, ABI3, and TREM2 implicate microglial-mediated innate immunity in Alzheimer's disease. Nat. Genet 49, 1373–1384 (2017). [PubMed: 28714976]
24. Dalmasso MC et al. Transethnic meta-analysis of rare coding variants in PLCG2, ABI3, and TREM2 supports their general contribution to Alzheimer's disease. Transl. Psychiatry 9, 55 (2019). [PubMed: 30705288]
25. Haure-Mirande J-V et al. Integrative approach to sporadic Alzheimer's disease: deficiency of TYROBP in cerebral Aβ amyloidosis mouse normalizes clinical phenotype and complement subnetwork molecular pathology without reducing Aβ burden. Mol. Psychiatry 24, 431–446 (2019). [PubMed: 30283032]
26. Zhang B et al. Integrated systems approach identifies genetic nodes and networks in late-onset Alzheimer's disease. Cell 153, 707–720 (2013). [PubMed: 23622250]
27. Han SH et al. Apolipoprotein E is present in hippocampal neurons without neurofibrillary tangles in Alzheimer's disease and in age-matched controls. Exp. Neurol 128, 13–26 (1994). [PubMed: 8070517]
28. Keren-Shaul H et al. A unique microglia type associated with restricting development of Alzheimer's disease. Cell 169, 1276–1290 (2017). [PubMed: 28602351]
29. Krasemann S et al. The TREM2-APOE pathway drives the transcriptional phenotype of dysfunctional microglia in neurodegenerative diseases. Immunity 47, 566–581 (2017). [PubMed: 28930663]
30. Zhou Y et al. Human and mouse single-nucleus transcriptomics reveal TREM2-dependent and TREM2-independent cellular responses in Alzheimer's disease. Nat. Med 26, 131–142 (2020). [PubMed: 31932797]
31. Srinivasan K et al. Untangling the brain's neuroinflammatory and neurodegenerative transcriptional responses. Nat. Commun 7, 11295 (2016). [PubMed: 27097852]
32. Kang SS et al. Microglial translational profiling reveals a convergent APOE pathway from aging, amyloid, and tau. J. Exp. Med 215, 2235–2245 (2018). [PubMed: 30082275]
33. Heneka MT et al. Neuroinflammation in Alzheimer's disease. Lancet Neurol. 14, 388–405 (2015). [PubMed: 25792098]
34. Perry VH & Holmes C Microglial priming in neurodegenerative disease. Nat. Rev. Neurol 10, 217–224 (2014). [PubMed: 24638131]
35. Ismail R et al. The relationships between neuroinflammation, beta-amyloid and tau deposition in Alzheimer's disease: a longitudinal PET study. J. Neuroinflammation 17, 151 (2020). [PubMed: 32375809]
36. Hashimoto T et al. Apolipoprotein E, especially apolipoprotein E4, increases the oligomerization of amyloid β peptide. J. Neurosci 32, 15181–15192 (2012). [PubMed: 23100439]
37. Hori Y, Hashimoto T, Nomoto H, Hyman BT & Iwatsubo T Role of apolipoprotein E in B-amyloidogenesis: isoform-specific effects on protofibril to fibril conversion of Aβ in vitro and brain Aβ deposition in vivo. J. Biol. Chem 290, 15163–15174 (2015). [PubMed: 25918154]
38. Liu C-C et al. ApoE4 accelerates early seeding of amyloid pathology. Neuron 96, 1024–1032 (2017). [PubMed: 29216449]
39. Hong S et al. Complement and microglia mediate early synapse loss in Alzheimer mouse models. Science 352, 712–716 (2016). [PubMed: 27033548]
40. Dejanovic B et al. Changes in the synaptic proteome in tauopathy and rescue of tau-induced synapse loss by C1q antibodies. Neuron 100, 1322–1336 (2018). [PubMed: 30392797]
41. Wu T et al. Complement C3 is activated in human AD brain and is required for neurodegeneration in mouse models of amyloidosis and tauopathy. Cell Rep. 28, 2111–2123 (2019). [PubMed: 31433986]
42. Shi Q et al. Complement C3 deficiency protects against neurodegeneration in aged plaque-rich APP/PS1 mice. Sci. Transl. Med 9, eaaf6295 (2017). [PubMed: 28566429]
43. Serrano-Pozo A, Frosch MP, Masliah E & Hyman BT Neuropathological alterations in Alzheimer disease. Cold Spring Harb. Perspect. Med 1, a006189 (2011). [PubMed: 22229116]

44. Stone DJ, Molony C, Suver C, Schadt EE & Potter WZ ApoE genotyping as a progression-rate biomarker in phase II disease-modification trials for Alzheimer's disease. Pharmacogenomics J. 10, 161–164 (2010). [PubMed: 19997085]
45. Yu L et al. APOE ε4, Alzheimer's disease pathology, cerebrovascular disease, and cognitive change over the years prior to death. Psychol. Aging 28, 1015–1023 (2013). [PubMed: 23647000]
46. Qian J, Betensky RA, Hyman BT & Serrano-Pozo A Association of APOE genotype with heterogeneity of cognitive decline rate in Alzheimer disease. Neurology 96, e2414–e2428 (2021). [PubMed: 33771840]
47. Guerreiro R et al. TREM2 variants in Alzheimer's disease. N. Engl. J. Med 368, 117–127 (2013). [PubMed: 23150934]
48. Jonsson T et al. Variant of TREM2 associated with the risk of Alzheimer's disease. N. Engl. J. Med 368, 107–116 (2013). [PubMed: 23150908]
49. Wang Y et al. TREM2-mediated early microglial response limits diffusion and toxicity of amyloid plaques. J. Exp. Med 213, 667–675 (2016). [PubMed: 27091843]
50. Parhizkar S et al. Loss of TREM2 function increases amyloid seeding but reduces plaque-associated ApoE. Nat. Neurosci 22, 191–204 (2019). [PubMed: 30617257]
51. Leyns CEG et al. TREM2 function impedes tau seeding in neuritic plaques. Nat. Neurosci 22, 1217–1222 (2019). [PubMed: 31235932]
52. Bemiller SM et al. TREM2 deficiency exacerbates tau pathology through dysregulated kinase signaling in a mouse model of tauopathy. Mol. Neurodegener 12, 74 (2017). [PubMed: 29037207]
53. Leyns CEG et al. TREM2 deficiency attenuates neuroinflammation and protects against neurodegeneration in a mouse model of tauopathy. Proc. Natl Acad. Sci. USA 114, 11524–11529 (2017). [PubMed: 29073081]
54. Gratuze M et al. Impact of TREM2R47H variant on tau pathology-induced gliosis and neurodegeneration. J. Clin. Invest 130, 4954–4968 (2020). [PubMed: 32544086]
55. Ulrich JD et al. ApoE facilitates the microglial response to amyloid plaque pathology. J. Exp. Med 215, 1047–1058 (2018). [PubMed: 29483128]
56. Serrano-Pozo A et al. Stable size distribution of amyloid plaques over the course of Alzheimer disease. J. Neuropathol. Exp. Neurol 71, 694–701 (2012). [PubMed: 22805771]
57. Haure-Mirande J-V et al. Deficiency of TYROBP, an adapter protein for TREM2 and CR3 receptors, is neuroprotective in a mouse model of early Alzheimer's pathology. Acta Neuropathol. 134, 769–788 (2017). [PubMed: 28612290]
58. Audrain M et al. Integrative approach to sporadic Alzheimer's disease: deficiency of TYROBP in a tauopathy mouse model reduces C1q and normalizes clinical phenotype while increasing spread and state of phosphorylation of tau. Mol. Psychiatry 24, 1383–1397 (2019). [PubMed: 30283031]
59. Audrain M et al. Reactive or transgenic increase in microglial TYROBP reveals a TREM2-independent TYROBP–APOE link in wild-type and Alzheimer's-related mice. Alzheimers Dement. 17, 149–163 (2021). [PubMed: 33314529]
60. Zhu Y et al. APOE genotype alters glial activation and loss of synaptic markers in mice. Glia 60, 559–569 (2012). [PubMed: 22228589]
61. Rodriguez GA, Tai LM, LaDu MJ & Rebeck GW Human APOE4 increases microglia reactivity at Aβ plaques in a mouse model of Aβ deposition. J. Neuroinflammation 11, 111 (2014). [PubMed: 24948358]
62. Ising C et al. NLRP3 inflammasome activation drives tau pathology. Nature 575, 669–673 (2019). [PubMed: 31748742]
63. Masuda T et al. IRF8 is a critical transcription factor for transforming microglia into a reactive phenotype. Cell Rep. 1, 334–340 (2012). [PubMed: 22832225]
64. Grubman A et al. A single-cell atlas of entorhinal cortex from individuals with Alzheimer's disease reveals cell-type-specific gene expression regulation. Nat. Neurosci 22, 2087–2097 (2019). [PubMed: 31768052]
65. Mathys H et al. Single-cell transcriptomic analysis of Alzheimer's disease. Nature 570, 332–337 (2019). [PubMed: 31042697]

66. Wan Y-W et al. Meta-analysis of the Alzheimer's disease human brain transcriptome and functional dissection in mouse models. Cell Rep. 32, 107908 (2020). [PubMed: 32668255]

67. Gosselin D et al. An environment-dependent transcriptional network specifies human microglia identity. Science 356, eaal3222 (2017). [PubMed: 28546318]

68. Friedman BA et al. Diverse brain myeloid expression profiles reveal distinct microglial activation states and aspects of Alzheimer's disease not evident in mouse models. Cell Rep. 22, 832–847 (2018). [PubMed: 29346778]

69. Gearing M, Rebeck GW, Hyman BT, Tigges J & Mirra SS Neuropathology and apolipoprotein E profile of aged chimpanzees: implications for Alzheimer disease. Proc. Natl Acad. Sci. USA 91, 9382–9386 (1994). [PubMed: 7937774]

70. Patrick E et al. Deconvolving the contributions of cell-type heterogeneity on cortical gene expression. PLoS Comput. Biol 16, e1008120 (2020). [PubMed: 32804935]

71. Wang X et al. Deciphering cellular transcriptional alterations in Alzheimer's disease brains. Mol. Neurodegener 15, 38 (2020). [PubMed: 32660529]

72. Zhang Y et al. Purification and characterization of progenitor and mature human astrocytes reveals transcriptional and functional differences with mouse. Neuron 89, 37–53 (2016). [PubMed: 26687838]

73. De Jager PL et al. A multi-omic atlas of the human frontal cortex for aging and Alzheimer's disease research. Sci. Data 5, 180142 (2018). [PubMed: 30084846]

74. Wang M et al. The Mount Sinai cohort of large-scale genomic, transcriptomic and proteomic data in Alzheimer's disease. Sci. Data 5, 180185 (2018). [PubMed: 30204156]

75. Mirra SS et al. The Consortium to Establish a Registry for Alzheimer's Disease (CERAD). Part II. Standardization of the neuropathologic assessment of Alzheimer's disease. Neurology 41, 479–486 (1991). [PubMed: 2011243]

76. Braak H & Braak E Neuropathological stageing of Alzheimer-related changes. Acta Neuropathol. 82, 239–259 (1991). [PubMed: 1759558]

77. Wang B et al. Similarity network fusion for aggregating data types on a genomic scale. Nat. Methods 11, 333–337 (2014). [PubMed: 24464287]

78. Ritchie ME et al. limma Powers differential expression analyses for RNA-sequencing and microarray studies. Nucleic Acids Res. 43, e47 (2015). [PubMed: 25605792]

79. Benjamini Y & Hochberg Y Controlling the false discovery rate: a practical and powerful approach to multiple testing. J. R. Stat. Soc. Series B Stat. Methodol 57, 289–300 (1995).

80. Huynh T-PV et al. Lack of hepatic apoE does not influence early Aβ deposition: observations from a new APOE knock-in model. Mol. Neurodegener 14, 37 (2019). [PubMed: 31623648]

81. Jankowsky JL et al. Mutant presenilins specifically elevate the levels of the 42 residue beta-amyloid peptide in vivo: evidence for augmentation of a 42-specific gamma secretase. Hum. Mol. Genet 13, 159–170 (2004). [PubMed: 14645205]

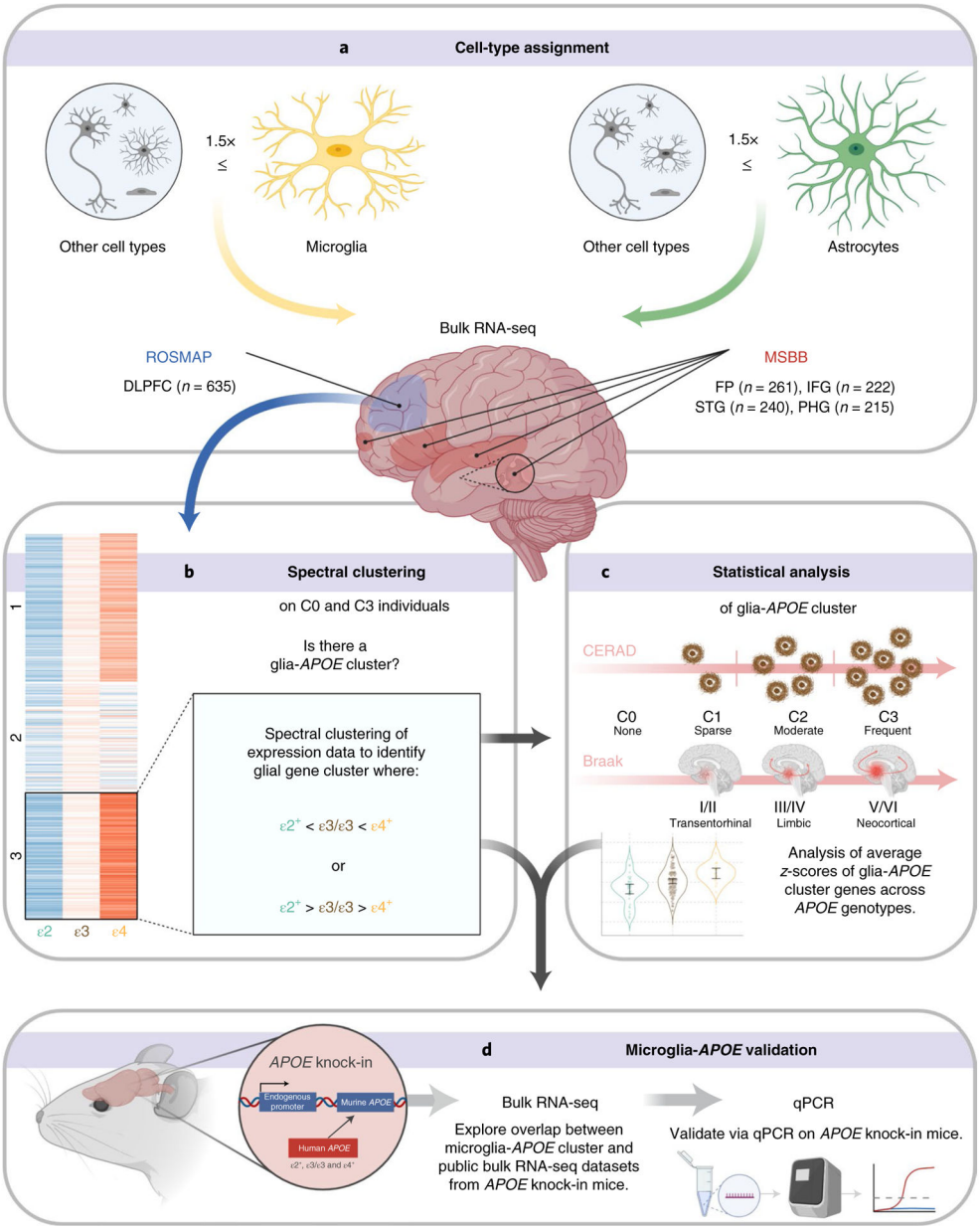

Fig. 1 |. Workflow of integrative analyses of *APOE* associations with microglia and astrocyte transcriptomic phenotypes.

a, Microglia- and astrocyte-predominant genes were defined as those whose expression is ≥1.5-fold in microglia or astrocytes, with respect to expression in all other cell types (neurons, oligodendrocytes, endothelial cells; and astrocytes or microglia, respectively), based on a public cell-type-specific RNA-seq database. Public bulk RNA-seq databases from ROSMAP DLPFC and MSBB STG, IFG, PHG and FP were interrogated for expression levels of these microglia- and astrocyte-predominant genes across *APOE* alleles (($\varepsilon2^+$: ε2/ε2, ε2/ε3); (ε3: ε3/ε3); ($\varepsilon4^+$: ε2/ε4, ε3/ε4, ε4/ε4)) and CERAD NP scores (C0, none; C1, sparse; C2, moderate; C3, frequent). **b**, Spectral clustering of group averaged *z*-scores of gene expression levels enabled the identification of gene clusters that follow an ε2 > ε3 > ε4 or an ε2 < ε3 < ε4 pattern in subjects without NPs (C0) and with frequent NPs (C3),

supporting an association with the *APOE* genotype that is independent of *APOE* effects on AD neuropathological changes. **c**, Statistical analyses were performed to test whether cluster genes are differentially expressed between *APOE*ε2 carriers, *APOE*ε4 carriers and A*POE*ε3 homozygotes. **d**, *APOE*-associated genes obtained from human transcriptomic datasets were cross-validated in mouse *APOE* knock-in mice expressing different human *APOE* alleles in the mouse *Apoe* locus, by both RT–qPCR and analysis of publicly available transcriptomic datasets from these mice.

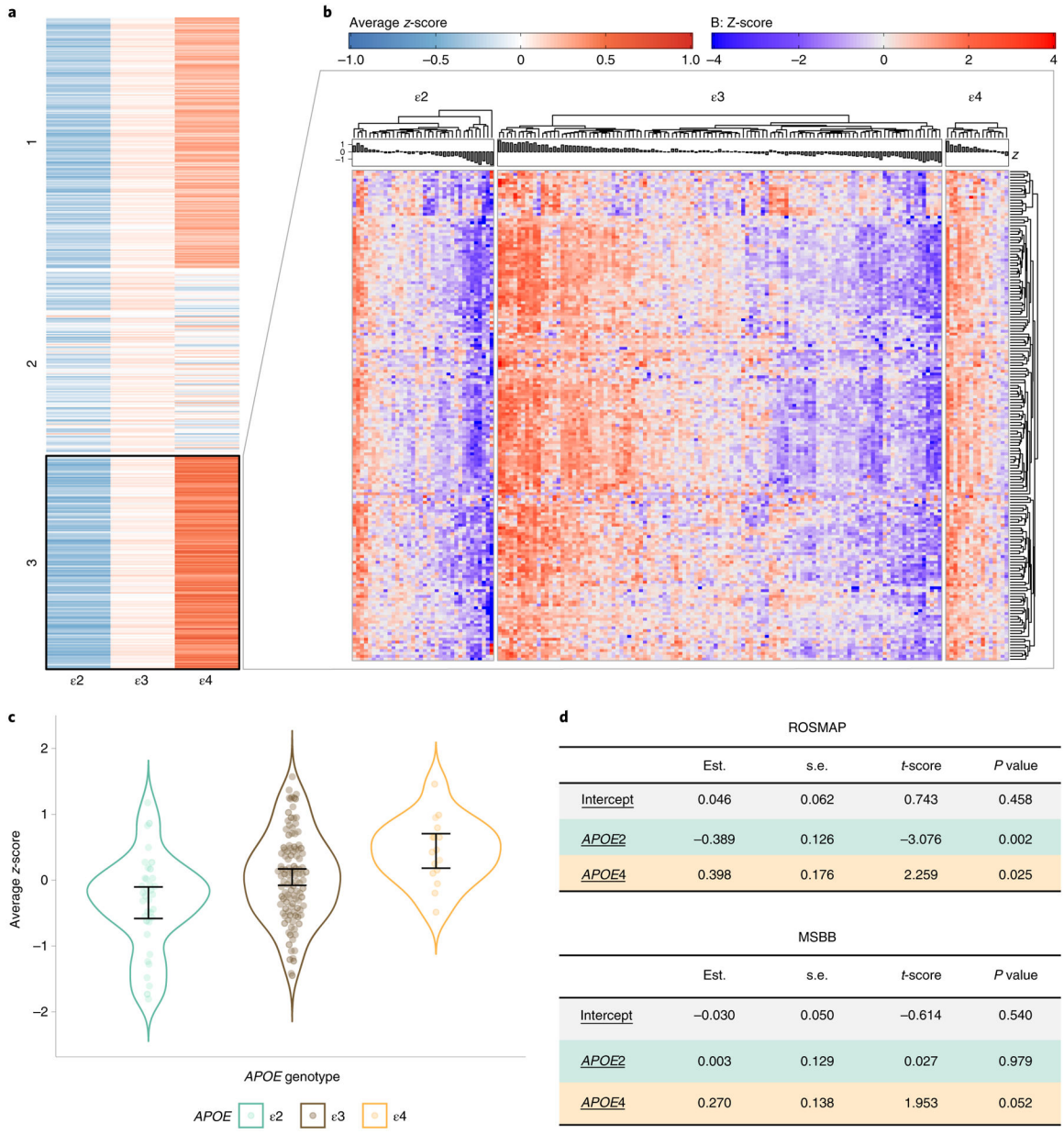

Fig. 2 |. Identification of a microglial gene signature associated with *APOE* genotype in normal aging.

a, Spectral clustering of group averaged expression-level *z*-score for each of 519 microglia-predominant genes in ROSMAP subjects with no NPs (CERAD 0), split by *APOE* group. **b**, Heatmap showing detail of the expression level of cluster 2 genes from **a** for all ROSMAP DLPFC C0 subjects, by *APOE* group ($n = 36$ *APOE*ε2 carriers, $n = 113$ *APOE*ε3 homozygotes, $n = 16$ *APOE*ε4 carriers). Note that the 172 genes of this microglia-*APOE* cluster overall have higher expression levels in *APOE*ε4 and lower in *APOE*ε2 carriers relative to *APOE*ε3 homozygotes, who have substantial interindividual variability. **c**, Violin plots showing average expression-level *z*-score of the 172 genes of the microglia-*APOE* cluster in each subject, by *APOE* group. Error bars represent the lower and upper 95% normal confidence limits of the sample mean based on the *t*-distribution. **d**, Statistical

analysis of the microglia-*APOE* cluster by *APOE* group in ROSMAP and MSBB subjects from all brain regions. The average *z*-scores of cluster genes were tested using a linear model. Estimated coefficient (est.), standard error (s.e.m.), *t*-score and corresponding two-sided *P* value are represented.

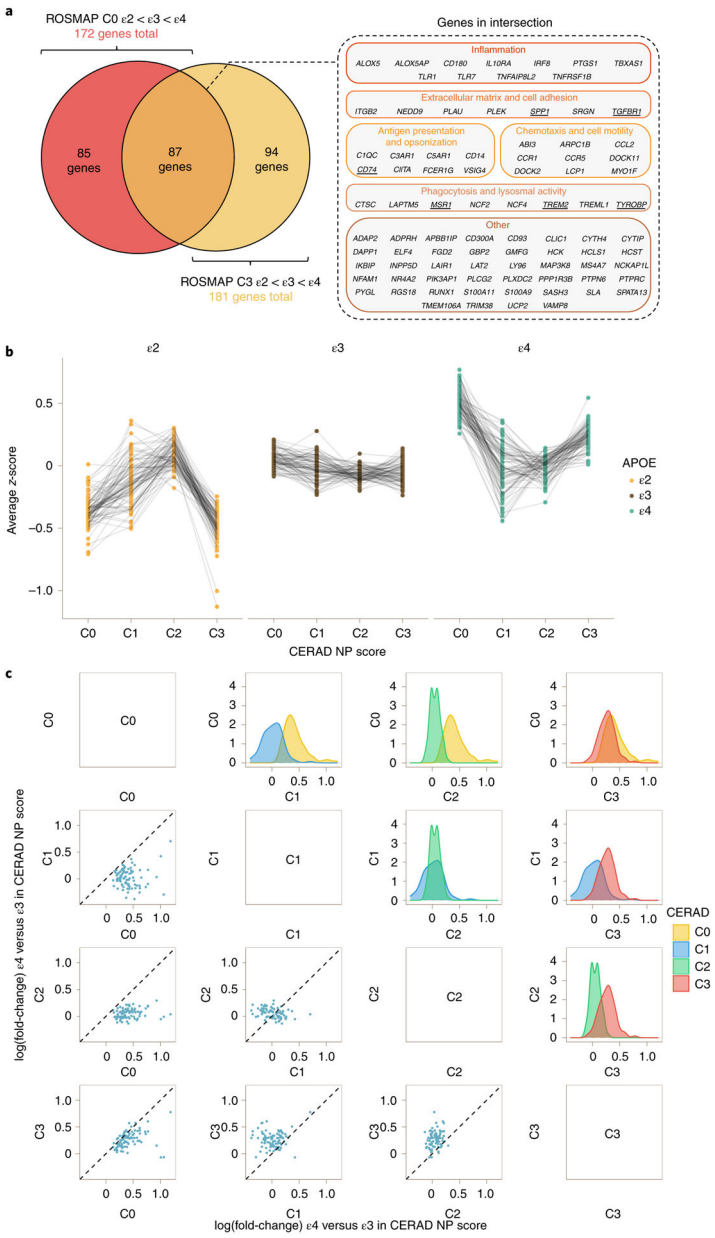

Fig. 3 |. The microglia-*APOE* signature is independent of known *APOE* effects on AD neuropathological changes.

a, Venn diagram (left) showing intersection between the 172 genes from the microglia-*APOE* cluster obtained by spectral clustering in ROSMAP C0 subjects and the 181 genes from C3 subjects. Note that the 87 DEGs in the intersection included relevant phagocytic and proinflammatory genes (right). The underlined genes were subsequently tested by RT–qPCR in *APOE* knock-in mice. **b**, Dot plots with connecting lines depicting group averaged expression-level *z*-scores of the 87 genes from **a** split by CERAD NP score and *APOE* genotype. Note that the most prominent changes across *APOE* genotypes correspond to C0 (no NPs) and C3 (frequent NPs) subjects. **c**, Correlation matrix comparing the *APOE*ε4 versus *APOE*ε3 change in expression levels (log(fold-change)) of the 87 DEGs from the microglia-*APOE* cluster of C0 and C3 subjects in the ROSMAP cohort. The scatter dot

plots on the left and density plots on the right demonstrate that the largest differences between *APOE*ε4 carriers and *APOE*ε3 homozygotes are observed in C1 (sparse NPs) and C2 (moderate NPs) versus both C0 (no NPs) and C3 (frequent NPs) subjects. By contrast, *APOE*ε4 versus *APOE*ε3 differences in expression levels were attenuated between C1 (sparse NPs) and C2 (moderate NPs) subjects, and between C0 (no NPs) and C3 (frequent NPs) subjects, suggesting either higher heterogeneity in microglial activation state in intermediate stages (C1 and C2) masking *APOE* genotype effects, or two waves of activation of this microglial transcriptional program (in C0 and C3).

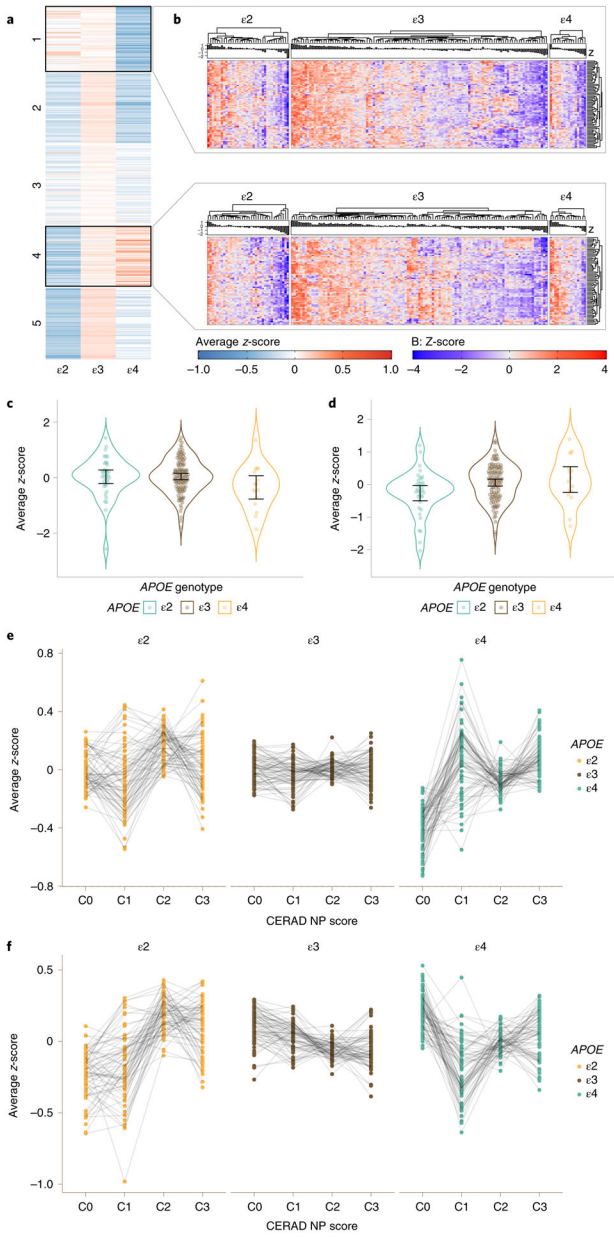

Fig. 4 |. Astrocyte transcriptomic changes associated with *APOE* genotype in normal aging.
a, Spectral clustering of subject group averaged expression-level *z*-score for each of 397 astrocyte-predominant genes in ROSMAP subjects with no neuritic plaques (CERAD 0), split by *APOE* group (ε2: ε2/ε2 + ε2/ε3; ε3: ε3/ε3; and ε4: ε2/ε4 + ε3/ε4 + ε4/ε4). **b**, Heatmap showing detail of the expression level of cluster 1 and 4 genes from **a** for all individuals of each *APOE* group. Note that the 69 genes of cluster 1 overall have higher expression levels in *APOE*ε2 and lower in *APOE*ε4 carriers relative to *APOE*ε3 homozygotes, whereas the 75 genes of cluster 4 overall have higher expression levels in *APOE*ε4 and lower in *APOE*ε2 carriers relative to *APOE*ε3 homozygotes. **c**,**d**, Violin plots showing group averaged expression-level *z*-score of the 69 genes of cluster 1 (**c**) and the 75 genes of cluster 4 (**d**) for all ROSMAP DLPFC C0 subjects, by *APOE* group (*n* =

36 *APOE*ε2 carriers, $n = 113$ *APOE*ε3 homozygotes, $n = 16$ *APOE*ε4 carriers). Error bars indicate the sample mean ±95% normal confidence limits based on *t*-distribution. **e**, Dot plots with connecting lines depicting group averaged expression-level *z*-scores of the 69 genes from cluster 1 in the ROSMAP cohort, split by CERAD NP score and *APOE* genotype. **f**, Dot plots with connecting lines depicting group averaged expression-level *z*-scores of the 75 genes from cluster 4 in the ROSMAP cohort, split by CERAD NP score and *APOE* genotype. Note that there is much more interindividual variability and more variability across *APOE* groups compared to the microglia-*APOE* cluster.

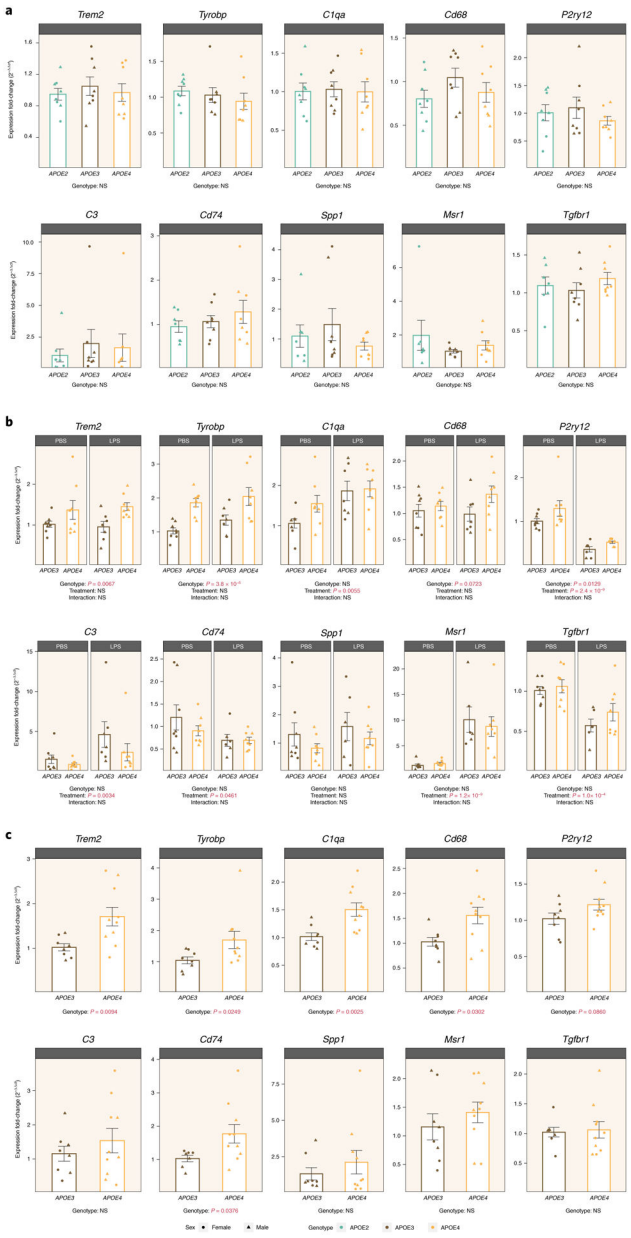

Fig. 5 |. Cross-validation of microglia-*APOE* cluster in *APOE* knock-in mice.

a, Bar graphs of relative quantification ($2^{-\Delta\Delta Ct}$) showing mean ± s.e.m. of the expression levels of relevant microglial (underlined in Fig. 3a) and astrocyte genes across 10–12-month-old *APOE*2 ($n = 8$), *APOE*3 ($n = 8$) and *APOE*4 ($n = 8$) knock-in mice, and the results of one-way ANOVA with Tukey's post hoc tests. Outliers in ΔCt values were detected and discarded from statistical analyses in *Clu*, *huAPOE* and *Msr1*. **b**, Bar graphs of relative quantification ($2^{-\Delta\Delta Ct}$) showing mean ± s.e.m. of the expression levels of relevant genes across $n = 15$ biologically independent *APOE*3 and $n = 17$ biologically independent *APOE*4 knock-in mice treated with either PBS or LPS, and the results of two-way ANOVA with genotype, treatment and genotype × treatment interactions. Outliers in ΔCt values were detected and discarded from statistical analyses in *C1qa*, *Cx3cr1* and *Tgfbr1*. **c**, Bar graphs

of relative quantification ($2^{-\Delta\Delta Ct}$) showing mean ± s.e.m. of the expression levels of relevant genes across *APP/PS1* mice crossed with *APOE*3 ($n = 8$) and *APOE*4 ($n = 10$) knock-in mice, and the results of one-way ANOVA with Tukey's post hoc tests. Outliers in ΔCt values were detected and removed from statistical analyses in *Clu*, *Gfap* and *Tyrobp*. NS, non-significant.

Table 1 |

Demographic characteristics and neuropathological findings across *APOE* groups in the ROSMAP cohort

	ε2	ε3	ε4
Age at death, years (mean ± s.d.)	87.9 ± 5.4	87.0 ± 4.8	87.1 ± 4.6
Sex, *n* female (%)	63 (72.4)	242 (62.7)	102 (63.0)
Years of education (mean ± s.d.)	15.7 ± 3.0	16.4 ± 3.6	16.7 ± 3.4
CERAD NP score, *n* (%)			
C0	36 (41.4)	113 (29.3)	16 (9.9)
C1	12 (13.8)	43 (11.1)	12 (7.4)
C2	28 (32.2)	136 (35.2)	54 (33.3)
C3	11 (12.6)	94 (24.4)	80 (49.4)
Braak NFT stage, *n* (%)			
Braak 0/I/II	17 (19.5)	73 (18.9)	20 (12.3)
Braak III/IV	65 (74.7)	241 (62.4)	81 (50.0)
Braak V/VI	5 (5.7)	72 (18.7)	61 (37.7)
Comorbid pathologies, *n* (%)			
Cerebral amyloid angiopathy (1/0/NA)	33 (37.9)/54 (62.1)/0 (0)	114 (29.5)/272 (70.5)/0 (0)	91 (56.2)/71 (43.8)/0 (0)
Arteriolosclerosis (1/0/NA)	47 (54)/39 (44.8)/1 (1.1)	151 (39.1)/232 (60.1)/3 (0.8)	61 (37.7)/100 (61.7)/1 (0.6)
Lewy body pathology (1/0/NA)	12 (13.8)/73 (83.9)/2 (2.3)	79 (20.5)/293 (75.9)/14 (3.6)	38 (23.5)/116 (71.6)/8 (4.9)
TDP-43 pathology (1/0/NA)	37 (42.5)/41 (47.1)/9 (10.3)	167 (43.3)/187 (48.4)/32 (8.3)	85 (52.5)/58 (35.8)/19 (11.7)
Hippocampal sclerosis (1/0/NA)	7 (8)/79 (90.8)/1 (1.1)	19 (4.9)/364 (94.3)/3 (0.8)	21 (13)/140 (86.4)/1 (0.6)

Cerebral amyloid angiopathy: 0, none/mild; 1, moderate/severe; NA, missing or unknown. Arteriolosclerosis: 0, none/mild; 1, moderate/severe; NA, missing or unknown. Lewy body pathology: 0, not present; 1, present, NA, missing or unknown. TDP-43 pathology: 0, none; 1, present; NA, missing or unknown. Hippocampal sclerosis: 0, not present; 1, present; NA, missing or unknown.